Published in Solar Energy Materials and Solar Cells 79, issue 4, 425-438, 2003
which should be used for any reference to this work

Thin film silicon solar cells for space applications: Study of proton irradiation and thermal annealing effects on the characteristics of solar cells and individual layers

J. Kuendig[a,*], M. Goetz[a], A. Shah[a], L. Gerlach[b], E. Fernandez[b]

[a] *Institute of Microtechnology (IMT), Thin-film silicon and Photovoltaic group, University of Neuchâtel, A.-L. Breguet 2, 2000 Neuchâtel, Switzerland*
[b] *ESA-ESTEC, Keplerlaan 1, NL 2200 AG Noordwijk, The Netherlands*

Abstract

The paper reports on the effects of a proton irradiation campaign on a series of thin-film silicon solar cells (single- and double-junction). The effect of subsequent thermal annealing on solar cells degraded by proton irradiation is investigated. A low-temperature annealing behaviour can be observed (at temperatures around 100 to 160°C) for microcrystalline silicon solar cells. To further explore this effect, a second proton irradiation campaign has been carried out, but this time on microcrystalline silicon layers. The effect of proton irradiation and subsequent thermal annealing on the optical and electronic properties of microcrystalline silicon is, thus, thoroughly investigated.

Keywords: Thin film solar cell; Microcrystalline; Proton irradiation; Annealing

1. Introduction

Solar cells in space are highly exposed to proton radiation. It has been shown that CIS [1] and thin-film amorphous silicon [2] solar cells have far higher radiation hardness when compared to conventional Si and GaAs devices. The power/weight ratio of thin-film solar cells is very promising for space applications, where weight is

*Corresponding author.
E-mail address: jamil.kuendig@unine.ch (J. Kuendig).
URL: http://www-micromorph.unine.ch.

an important factor influencing launching costs. Thin-film double-junction solar cells using amorphous silicon (a-Si:H) and microcrystalline silicon (μc-Si:H), i.e. the so-called "micromorph" tandem cells [3–6], are a further interesting candidate for use on satellites, but the proton radiation hardness of the microcrystalline material had so far not been thoroughly explored. The present paper intends to fill this gap, by reporting on corresponding proton irradiation tests and subsequent annealing experiments. We thereby will complete the experimental data already reported by us in conference papers [7–9] and give a tentative interpretation of the observed effects. Our test samples are thin-film silicon solar cells (both amorphous and microcrystalline) as well as individual microcrystalline silicon layers.

2. Experimental

2.1. Sample details

2.1.1. Solar cells

For the solar cell samples, single- and double-junction devices have been studied. All cells were manufactured by the very high frequency glow-discharge (VHF-GD) technique [10] at IMT Neuchâtel.

As for single-junction cells, we have irradiated thin-film n–i–p a-Si:H and n–i– p μc-Si:H solar cells. W.r.t. double-junction tandem devices, both n–i–p and p–i–n micromorph (μc-Si:H/a-Si:H) solar cells (structure illustrated in Fig. 1) were irradiated.

Different substrates were chosen for the single-junction a-Si:H n–i–p solar cells: glass, stainless steel sheet metal, and polyimide. The preirradiation conversion efficiency varied from 7.5% to 8.5% for the a-Si:H cells. Glass was the substrate used for all other cells tested (n–i–p μc-Si:H, n–i–p micromorph and p–i–n micromorph). For the double-junction p–i–n micromorph cells, the preirradiation conversion efficiency was between 10% and 11%. Prior to starting the series of irradiations, all cells have been annealed at 180°C for 90 minutes.

2.1.2. Microcrystalline layers

We have also studied the effect of proton irradiation on undoped hydrogenated microcrystalline silicon (μc-Si:H) layers that were manufactured by the VHF-GD

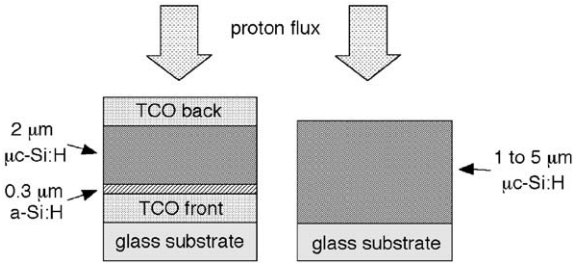

Fig. 1. Basic structure of p–i–n micromorph silicon solar cell (left) and μc-Si:H layer (right).

technique [10] at IMT Neuchâtel. These layers were deposited with 5% concentration of silane in hydrogen. A gas purifier was used to avoid oxygen contamination leading to unintentional doping effects and, thus, to obtain nearly intrinsic μc-Si:H layers.

We have studied 5 samples of different thicknesses, varying from 1 to 5 μm by steps of 1 μm. Each layer was deposited on two substrates: glass and silicon wafer. As in the case of cells, all layers were annealed at 180°C for 90 min prior to starting the series of irradiations.

2.2. Irradiation technique

Our samples were irradiated by the European Space Agency (ESA) at CEA (Paris), using a rocking equipment described hereafter. The samples' substrates were placed on a 5 mm aluminium holder, so that no proton entered the cell or the layer through the substrate side. A 500 μm aluminium sheet was applied at the top of the samples, and the whole equipment was rotating compared to the proton flux. This was used to reduce the initial energy of the protons (10 MeV) to a lower value (from several tenths of keV up to 5 MeV). The fluence (dose of particles per area) was 1.5E13 p^+/cm^2. The obtained energy spectrum of the incident protons has been calculated and is shown in Fig. 2. The initial energy of the protons had to be reduced below 10 MeV, as protons of this energy pass through thin-film solar cells or layers without being absorbed. All cells were irradiated under open-circuit conditions.

After irradiation, annealing steps at increasing temperatures have been carried out on all the samples.

2.3. Experimental techniques

2.3.1. Solar cells

The cells were characterized before and after irradiation, and after each of the post-irradiation annealing steps. This was done at IMT with a solar simulator under

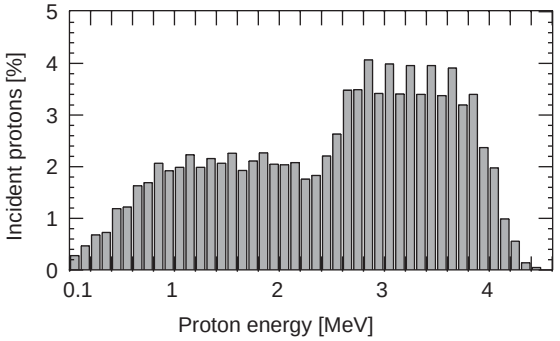

Fig. 2. Energy spectrum of the incident protons.

AM1.5 conditions (1000 W/m^2, terrestrial standard test conditions) and with Spectral Response measurements. Three parameters were measured: the open-circuit voltage (V_{oc}), the short-circuit current (I_{sc}), and the fill factor (FF). A fourth parameter is calculated: the efficiency (η). It is equal to the product of V_{oc}, I_{sc} and FF (if these three parameters are measured under AM1.5 conditions, which is here the case). The difference for AM0 (space) conditions (illumination in space: 1360 W/m^2) is found, by calculation from a typical spectral response curve of an amorphous cell, to be an increase by 22% of I_{sc}; one should expect also a minor increase in V_{oc} and a small reduction of FF and η. Comparisons are made w.r.t. the mean value of the normalized conversion efficiency of four to six cells from the same substrate for each type of solar cells.

2.3.2. Microcrystalline layers

The μc-Si:H layers have been characterized before and after irradiation, and after each of the post-irradiation annealing steps. As we are interested in the possible changes in structural, optical and electronic properties of the layers, several measurements were carried out: infrared transmission (IR), photothermal deflection spectroscopy (PDS), constant photocurrent method (CPM), dark conductivity, steady-state photoconductivity (SSPC) and steady-state photoconductivity grating (SSPG). The following parameters were considered in order to evaluate the influence of proton irradiation: subbandgap absorption coefficient α [cm^{-1}] measured by PDS and CPM, mobility-recombination time ($\mu^0\tau^R_{min}$) product of the minority carriers (holes) as yielded by the SSPG method, mobility-recombination time ($\mu^0\tau^R_{maj}$) product of the majority carriers (electrons) as yielded by measurement of the photoconductivity, and dark conductivity σ_{dark}. By combining the SSPG and photoconductivity measurements, according to [11–12], one can deduce a parameter b that is proportional to the ratio of majority carrier density to minority carrier density. The parameter b is, thus, a sensitive indication of the position of the Fermi level. Also determined according to [11–12] was the value $\mu^0\tau^0$, a mobility-lifetime product that is normalized in such a way as to be independent of the Fermi level.

3. Results and discussion

3.1. Solar cells

For all three types of n–i–p a-Si:H silicon solar cells (on polyimide, stainless steel sheet-metal and glass substrates), an excellent radiation hardness has been observed. No difference was observed for the different substrates. The results show that these cells are only very slightly damaged by proton irradiation at the chosen fluence and energy. For the n–i–p μc-Si:H and n–i–p micromorph silicon solar cells, all parameters show a loss after the proton irradiation. After thermal annealing however, the four parameters reach again their initial value (i.e. the value before irradiation). Fig. 3 presents the normalized efficiency of n–i–p a-Si:H, n–i–p μc-Si:H and n–i–p micromorph solar cells on glass substrates after proton irradiation and

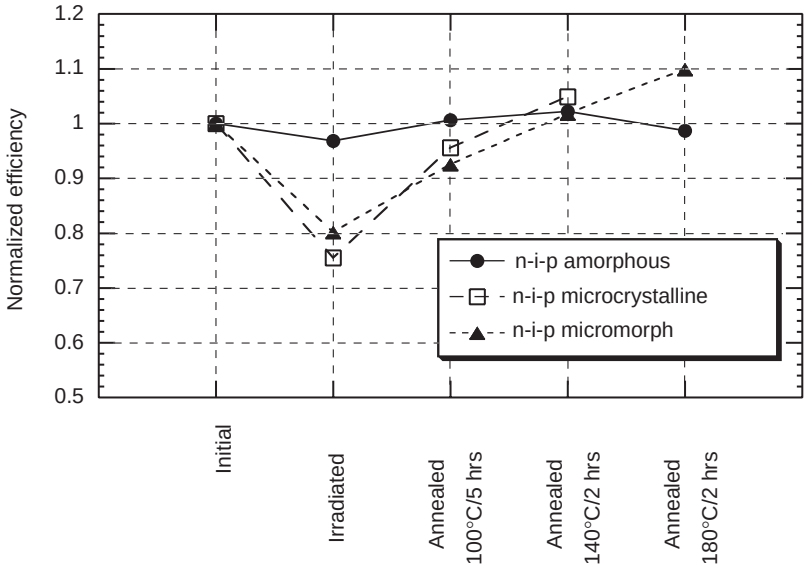

Fig. 3. Normalized efficiencies of n–i–p a-Si:H, n–i–p μc-Si:H and n–i–p micromorph solar cells on glass substrates. The datapoints are averaged curves, averaged over 4 cells, on the same substrate.

also after subsequent annealing at different temperatures (100°C for 5 h, 140°C for 2 h, 180°C for 2 h). Each data point is a mean value of four solar cells on the same glass substrate. All n–i–p cells were irradiated through the p-side, with proton flux passing first through front TCO before reaching the p-layer.

The normalized efficiency of p–i–n micromorph (Fig. 4) solar cells looks quite similar with the one of n–i–p micromorph solar cells (Fig. 3). The annealing time and temperature are the same for both types of cells (p–i–n and n–i–p micromorph). As shown in Fig. 4, the degradation due to proton bombardment could be partly recovered with post-irradiation isothermal annealings. Irradiation results of two different substrates are illustrated in Fig. 4, and each data point is a mean value of four solar cells on the same substrate. Note that the p–i–n micromorph solar cells were irradiated through the n-side, with proton flux passing first through back TCO before reaching the n-layer.

As the normalized conversion efficiency of n–i–p μc-Si:H and of n–i–p micromorph silicon solar cells looks similar after proton irradiation and after the different annealing steps (see Fig. 3), we supposed that it is the μc-Si:H cell of the micromorph tandem solar cell that was damaged by the irradiation. This is confirmed by relative spectral response measurements made on a p–i–n micromorph tandem solar cell.

Fig. 5 shows clearly that it is the microcrystalline (bottom) cell that is damaged after the proton irradiation. At the beginning, we had two hypotheses to explain this observation. Firstly, an explanation could be proposed in the different thicknesses of the amorphous and microcrystalline layers of the tandem micromorph cell. As the

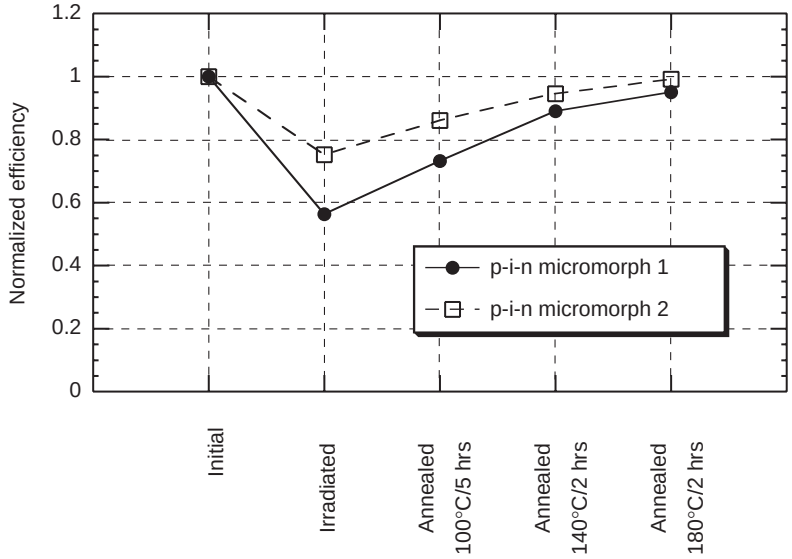

Fig. 4. Normalized efficiencies of p–i–n micromorph solar cells on glass substrates during a first cycle of irradition and subsequent annealing steps.

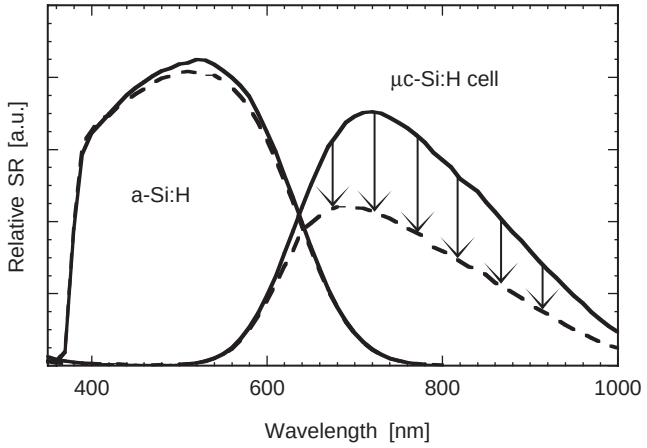

Fig. 5. Relative spectral response [a.u.] versus wavelength [nm] for a p–i–n micromorph cell (dotted line = measurement after proton irradiation).

microcrystalline layers (bottom cell) are about five times thicker than the amorphous layers (top cell), there is much more risk to find damages located in the microcrystalline layers. This hypothesis will, however, be at least partly contradicted by the thickness dependence of radiation damage observed for individual layers (Section 3.2). A second explanation could be found in the fact that amorphous material has originally already a high density of defects. The fact that a-Si:H solar

cells are, therefore, designed to work with these defects could also explain that amorphous layers are much more radiation-resistant than microcrystalline layers. A further possible explanation based on the presence and spatial distribution of hydrogen in the two different types of material is given, as a conjecture, in Section 4.3 hereafter.

The p–i–n micromorph solar cells whose radiation results are illustrated in Fig. 4 have been exposed a second time to the exactly same proton irradiation. After this second bombardment, we have annealed the samples at significantly lower temperatures (70°C, 100°C, and 130°C, each annealing step during 10 h). Experimental results of the same two samples are illustrated in Fig. 6. It shows that after annealing at lower temperatures the degradation due to proton bombardment could also be partly recovered. We expect that longer annealing times at low temperatures around 70 to 100°C may allow for a full recovery of the degradation. It is likely that a steady state would be reached in space, where simultaneous degradation and annealing come to a balance.

We were indeed surprised to discover this low temperature annealing behaviour for our thin-film microcrystalline silicon solar cells. We concluded that there was a great interest to understand in more detail what happens in the intrinsic layer itself during the irradiation. So a new proton irradiation campaign was carried out, but this time on individual intrinsic microcrystalline layers.

3.2. Microcrystalline layers

As we have seen in the section on solar cell results (Section 3.1), the amorphous silicon solar cells have a good proton radiation hardness, which is not the case for

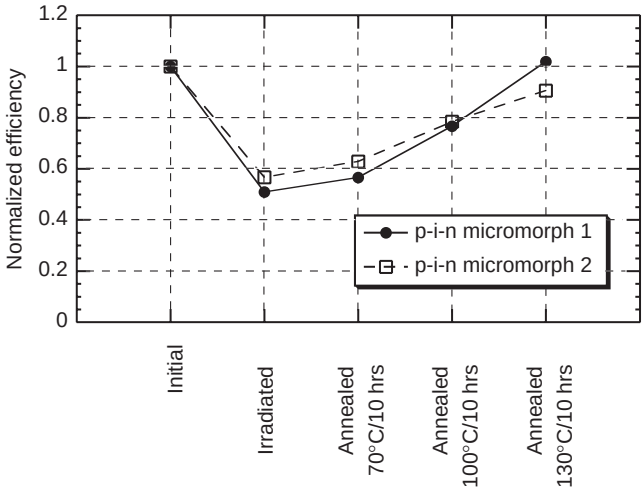

Fig. 6. Normalized efficiencies of p–i–n micromorph solar cells on glass substrates during a second cycle of irradiation and subsequent annealing steps, with lower annealing temperatures than those used in the first cycle.

microcrystalline silicon solar cells. A further irradiation campaign, on microcrystalline layers of different thicknesses (5 layers: 1, 2, 3, 4 and 5 μm thick), has therefore been carried out in order to check if there is any thickness dependency of the effects of irradiation on microcrystalline layers. Furthermore, we are interested in the change of the optical and electronic properties, and their relation to the density of defects. Each characterization measurement was done at several distinct moments for each layer: immediately after the deposition process, after the irradiation (for irradiated samples and also for non-irradiated samples used as a control group), and after each subsequent thermal annealing step (for irradiated samples only).

In the infrared transmission measurements, we have not at all seen any significant changes between the values before and after proton irradiation (not illustrated). This means that there is no detectable change in the structure of the μc-Si:H material after the irradiation process.

Concerning the PDS and CPM measurements, we have seen after irradiation an increase of the absorption coefficient α by a factor 1.5–2 in the 0.7–0.9 eV energy range. This means that, with the irradiation, we have created deep defects in the mid-gap region.

With the thermal annealing steps (at 70°C, 100°C and 130°C: each step during 10 h; and 160°C during 50 h), we did not remark any recovery until the 160°C step. After this last step, however, the absorption measurements yielded nearly the same value as before irradiation (see Fig. 7). So we can state that the defects created by proton irradiation could be almost fully recovered.

The $\mu^0\tau^R$ product of the minority and majority carriers is plotted in function of the parameter b (which represents the Fermi level position) in Fig. 8. Several observations can be made: first, we observe an increase of the parameter b with time after the manufacturing and before the irradiation. This is due to the unintentional incorporation of oxygen in the μc-Si:H layers (post-oxidation), which leads to n-type doping for microcrystalline silicon material. Secondly, we see that after irradiation the value of the parameter b drops significantly. This indicates that the irradiation creates deep defects (broken "bonds") which are electrically neutral and bring the Fermi level E_f towards the centre of the gap. Thirdly, the $\mu^0\tau^R_{maj}$ product of the majority carriers drops substantially during irradiation. As the mobility μ^0 can be assumed to remain constant, we deduce that $\tau^R{}_{maj\ irradiated} \ll \tau^R{}_{maj\ initial}$. This confirms the creation of neutral defects (D^0 defects). We can also remark that if the thickness of the layer is increased, the observed increase in defect density N_{D^0} due to irradiation is less pronounced.

After each of the thermal annealing steps (at 70°C, 100°C and 130°C, each step during 10 h, and at 160°C during 50 h), we can observe that the parameter b moves towards its original value (i.e. the value obtained after post-oxidation of the layer, i.e. just before irradiation). This behaviour can be seen in Fig. 9, representing the values of the 2 μm thick layer.

The "normalized" $\mu^0\tau^0$ product is plotted, in function of layer thickness, in Fig. 10. Here, μ^0 can be assumed to remain constant, and τ^0 can be assumed to be proportional to $N_{D^0}^{-1}$. After the irradiation, we observe that: (a) for the thinner layers (1, 2 and 3 μm thick), N_{D^0} is $\approx$1.7–1.8 times higher than before irradiation; (b) for

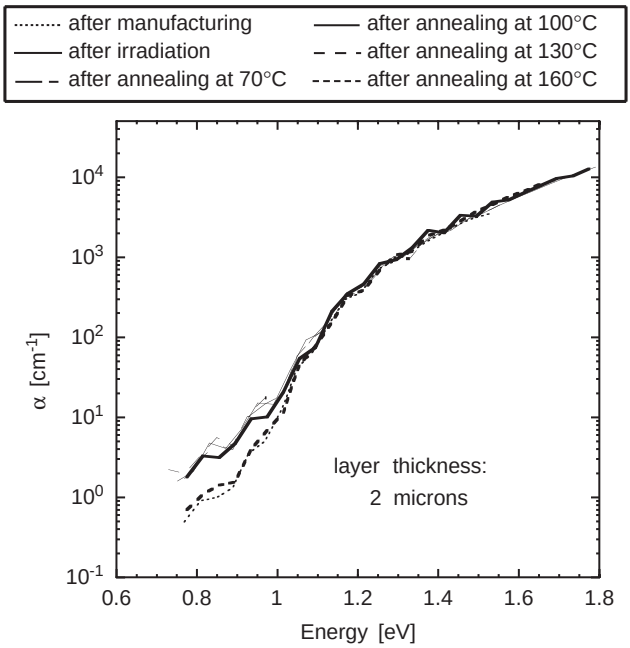

Fig. 7. Subbandgap absorption measurements (by CPM) on a 2 μm thick μc-Si:H layer.

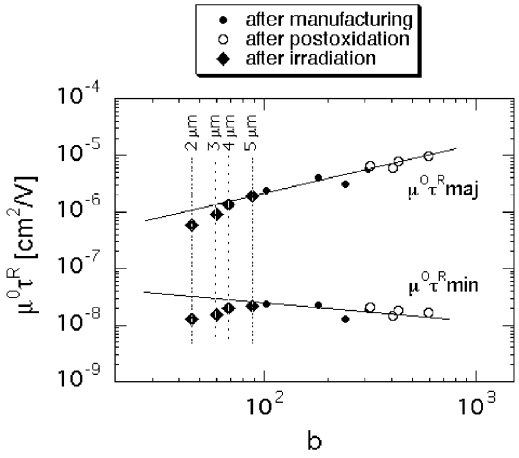

Fig. 8. $\mu\tau$ product of the minority and majority carriers plotted in function of the parameter b for the 2, 3, 4 and 5 μm thick μc-Si:H layers.

the thick layers (4 and 5 μm thick), N_{D^0} is ≈only 1.3–1.4 times higher than before irradiation. As the microcrystalline layer of the irradiated p–i–n micromorph tandem solar cells is about 2 to 3 μm thick, we observe a correlation between the electrical measurements on the cells (where $\eta_{\text{irradiated}}/\eta_{\text{initial}} = 0.5-0.7$) and the factor of

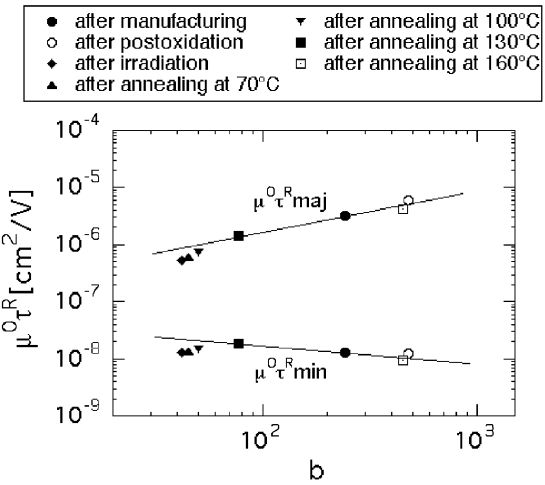

Fig. 9. $\mu\tau$ product of the minority and majority carriers plotted in function of the parameter b for the 2 μm thick μc-Si:H layer.

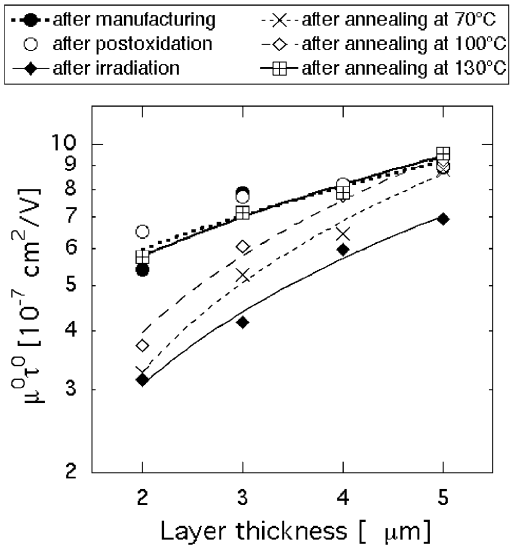

Fig. 10. $\mu^0\tau^0$ product plotted in function of the layer thickness for μc-Si:H layers.

increase for N_{D^0}; thereby: $\eta_{\text{irradiated}}/\eta_{\text{initial}} \propto N_D^{-1}$. This would mean that the defect density of the i-layer of is directly linked to the conversion efficiency of the cell. This can be easily understood, as with an increase of defect density we also have an increase in the density of recombination centres: electrical transport is impaired and

collection lengths are decreased, resulting in a corresponding drop in efficiency. But we have to be careful in our interpretation, because the electrical measurements made on the layers are coplanar measurements and therefore not directly relevant of the collection path in solar cells, due to a possible anisotropy of transport in μc-Si:H material.

After the thermal annealing step at 130°C, we can observe that the values fit already very well with those measured before irradiation (see Fig. 10). We can also remark that the thicker the layer is, the quicker it recovers (thickness dependency effect).

The dark conductivity σ_{dark} is plotted in function of the layer thickness in Fig. 11. We observe that before irradiation, σ_{dark} is relatively constant. After the irradiation meanwhile, there is a strong dependency between the layer thickness and the dark conductivity (thickness $\searrow$, σ_{dark} $\searrow$). The reason for this behaviour could be that during the irradiation we have a profile of defect generation ($N_D^{\text{close to the surface}} > N_D^{\text{deep}}$): as in all electrical measurements the current always chooses the less resistive path, we could now interpret this observation (thickness $\searrow$, σ_{dark} $\searrow$) as an effect of the layer thickness on the electrical measurements; the defect creation would thereby be mainly located in the upper part of the microcrystalline layer.

After all the thermal annealing steps, we can observe an almost full recovery of σ_{dark} (see Fig. 11). Like for the $\mu^0\tau^0$ plot (Fig. 10), we can remark, also for σ_{dark}, a thickness dependency effect during the thermal annealing steps. This can be explained with the assumed non-uniform defect profile.

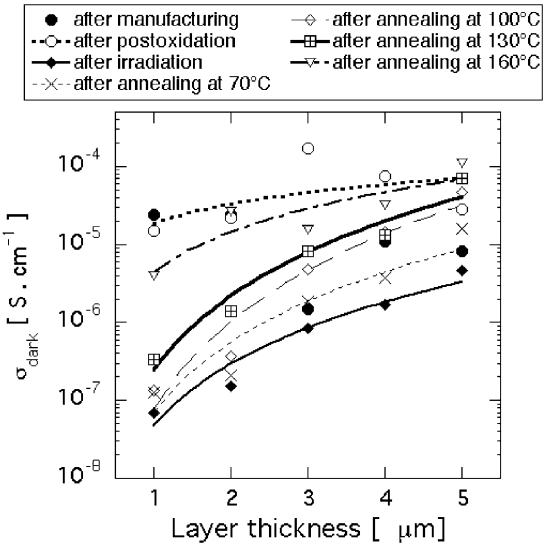

Fig. 11. Dark conductivity σ_{dark} plotted in function of the layer thickness for μc-Si:H layers.

4. Conclusions

4.1. Solar cell proton irradiation

For the solar cell irradiation part, we have seen that thin film amorphous silicon solar cells have an excellent radiation hardness. Thin-film microcrystalline and micromorph (μc-Si:H/a-Si:H tandem) solar cells show an important loss of conversion efficiency after proton irradiation. But almost the full loss of efficiency could be recovered after low-temperature annealing during a short time. In the tandem cell, it is the microcrystalline bottom cell that was mainly damaged by the proton irradiation.

The thermal history of the solar modules in space is very important, especially for "micromorph" tandem solar cells with their excellent power/weight potential. We contend that a steady state could be reached in space, where simultaneous radiation degradation and thermal annealing would come to a balance.

4.2. Microcrystalline layer proton irradiation

Concerning the irradiation of individual microcrystalline layers, the creation of neutral defects D^0 has been observed after irradiation. After the different thermal annealing steps, however, the initial properties of the layers could be recovered. The following explanations have been deduced from the experimental observations: first, the proton irradiation has generated a non-uniform defect profile. This means that there is, after irradiation, a higher defect density close to the surface than deep in the layer. Second, we observed a layer thickness effect on the coplanar electrical measurements. This can be easily understood with the fact that, during all electrical measurements, the current always takes the less resistive path. With the defect creation, the resistivity of the material is locally increased because the Fermi level is thereby shifted towards mid-gap. When performing coplanar electrical measurements on thicker layer, the current will, however, pass mainly through the less degraded regions that have a lower neutral defect density and, thus, a higher value of σ_{dark}; these regions are deeper in the layer, and, therefore, the measurements on thicker layers are mainly probing this region. Third, we could observe a correlation between the evaluated increase in defect density for a 2 μm thick layer and the measured decrease in efficiency for single-junction microcrystalline cells, so as to obtain $\eta_{\mathrm{irradiated}}/\eta_{\mathrm{initial}} \propto N_D^{-1}$. This would mean that the defect density of the microcrystalline i-layer is directly linked to the conversion efficiency of the cell.

4.3. Possible explanation of the irradiation and annealing effects

By proton irradiation, neutral defects D^0 were created in the microcrystalline silicon layers. From a physical point of view, one can assume that bonds previously saturated by hydrogen were broken and new dangling bonds were created. This process looks similar to the Staebler–Wronski effect as known for amorphous silicon material.

By thermal annealing, atomic hydrogen contained in the microcrystalline silicon material moves to the defect sites and passivates the broken bonds created by irradiation. The increase in temperature helps the atomic hydrogen to diffuse to the defect sites. The higher the annealing temperature, the more pronounced the thermal diffusion of atomic hydrogen will be.

The difference in radiation hardness between amorphous and microcrystalline thin-film silicon solar cells can now be attributed to a further possible explanation: for the amorphous silicon material, hydrogen is distributed in the material in a spatially homogeneous manner. So, defect passivation is easy, even at ambiant temperature. A kind of immediate self-passivation of defects would take place in amorphous silicon material. Unlike the situation in amorphous silicon material, hydrogen is not distributed spatially in a homogeneous manner in microcrystalline material. It is located at the grain boundaries and in the amorphous phases (between the microcrystalline grains). As there is in general very little atomic hydrogen located close to most radiation defects, which are, in their turn, located within the microcrystalline grains, it is very difficult to obtain defect passivation at ambient temperature. With thermal annealing, on the other hand, thermal diffusion of atomic hydrogen is greatly enhanced, so that defect passivation can take place.

5. Acknowledgments

The authors are grateful to Mr. A. Robben and P. Nieminen from ESTEC for their contributions to the proton irradiation tests and to the proton spectrum modelling. This work was partly supported by ESA-ESTEC. The authors are also grateful to N. Wyrsch, J. Meier, E. Vallat-Sauvain, P. Torres, J. Bailat, C. Droz, L. Feitknecht, P. Pernet and X. Niquille from IMT.

References

[1] H. Schock, K. Bogus, Proceedings of the Second WCPEC, 1998, pp. 3586–3589.
[2] S. Guha, J. Yang, A. Banerjee, T. Glatfelder, G.J. Vendura, A. Garcia, M. Kruer, Proceedings of the Second WCPEC, 1998, pp. 3609–3613.
[3] N. Wyrsch, P. Torres, M. Goetz, S. Dubail, L. Feitknecht, J. Cuperus, A. Shah, B. Rech, O. Kluth, S. Wieder, O. Vetterl, H. Stiebig, C. Beneking, H. Wagner, Proceedings of the Second WCPEC, 1998, pp. 467–471.
[4] J. Meier, H. Keppner, S. Dubail, Y. Ziegler, L. Feitknecht, P. Torres, Ch. Hof, U. Kroll, D. Fischer, J. Cuperus, J. A. Anna Selvan, A. Shah, Proceedings of the Second WCPEC, 1998, pp. 375–380.
[5] J. Meier, E. Vallat-Sauvain, S. Dubail, U. Kroll, J. Dubail, S. Golay, L. Feitknecht, P. Torres, S. Fay, D. Fischer, A. Shah, Sol. Energy Mater. Sol. Cells 66 (2001) 73–84.
[6] L. Feitknecht, O. Kluth, Y. Ziegler, X. Niquille, P. Torres, J. Meier, N. Wyrsch, A. Shah, Sol. Energy Mater. Sol. Cells 66 (2001) 397–403.
[7] J. Kuendig, M. Goetz, J. Meier, P. Torres, L. Feitknecht, P. Pernet, X. Niquille, A. Shah, L. Gerlach, E. Fernandez, Proceedings of the 16th EU PVSEC, 2000, pp. 986–989.

[8] J. Kuendig, M. Goetz, X. Niquille, A. Shah, S. Vaccaro, J. Mosig, L. Gerlach, P. de Maagt, E. Fernandez, Proceedings of the 28th IEEE PVSC, 2000, pp. 1079–1082.
[9] J. Kuendig, A. Shah, Proceedings of the 29th IEEE PVSC, 2002, pp. 974–977.
[10] H. Curtins, N. Wyrsch, A. Shah, Electron. Lett. 23 (1987) 228–230.
[11] N. Beck, N. Wyrsch, C. Hof, A. Shah, J. Appl. Phys. 79 (1996) 9361–9368.
[12] C. Droz, M. Goerlitzer, N. Wyrsch, A. Shah, J. Non-Cryst. Solids 266–269 (2000) 319–324.